Appl. Phys. B 50, 487–497 (1990)

Applied Physics B Photophysics and Laser Chemistry

Properties of Laser-Induced Stimulated Emission for Diagnostic Purposes*

U. Westblom[1], S. Agrup[1], M. Aldén[1], H. M. Hertz[1], and J. E. M. Goldsmith[2]

[1] The Combustion Center, Lund Institute of Technology, P.O. Box 118, S 221 00 Lund, Sweden

[2] Combustion Research Facility, Sandia National Laboratories, Livermore, CA 94551, USA

Received 26 December 1989/Accepted 8 February 1990

Abstract. We describe an experimental and semi-quantitative theoretical investigation of the characteristics of two-photon-induced stimulated emission related to diagnostic applications. The laser power dependence, pressure dependence, and the spectral shape of the stimulated emission signal in CO are discussed and compared with those for laser-induced fluorescence. We also discuss decreases in the laser-induced fluorescence signal caused by the stimulated emission process, and propose a method for providing increased spatial resolution in measurements made using stimulated emission detection.

PACS: 33.80.Wz, 42.55.Em, 82.40.Py

Since the advent of the laser in the early nineteen-sixties, a variety of laser-based spectroscopic techniques have been developed for diagnostic purposes. These methods are extremely valuable for probing harsh environments such as flames, where the nonintrusive nature and high spatial and temporal resolution obtainable with optical techniques are very useful. Spontaneous Raman scattering and coherent anti-Stokes Raman scattering (CARS) are commonly used for measurements of temperatures and major species concentrations, and laser-induced fluorescence (LIF) has been widely used for detecting minor species. For a comprehensive review of the application of these techniques to combustion diagnostics, see [1] and references therein.

In the field of laser-induced fluorescence, the use of multiphoton excitation schemes has made it possible to detect flame species that would otherwise require VUV excitation, such as O [2], H [3], and CO [4]. In diagnostic applications of multiphoton (as well as single-photon) LIF, it has been commonly thought that collision-induced processes and spontaneous emission generally dominate deexcitation from the laser-excited state. However, flame and cell experiments on atomic oxygen have recently shown that stimulated emission (SE) induced by two-photon laser excitation provides an additional deexcitation pathway [5]. After this demonstration, the effect has also been utilized for flame detection of carbon atoms [6], hydrogen atoms [7], and nitrogen atoms [8]. Similar effects have been observed earlier in many atomic and molecular species (see, for example, [9–12]). There seems to be some controversy and confusion over the origin of the emission, partly for semantic reasons. The process has been attributed to superradiance, superfluorescence, and amplified spontaneous emission (or stimulated emission). The difficulty of determining the origin of the process in a particular study has recently been demonstrated by the use of the description "bidirectional emission" in order not to give it an incorrect designation [13].

Superradiance (also called Dicke superradiance [14]) and superfluorescence are coherent radiation from a small volume of dipoles initially prepared with a large degree of coherence, where there is a strong coupling between the atoms through the common

* This work was supported by the Swedish National Board for Technical Developments, the Swedish Energy Administration, and the U.S. Department of Energy, Office of Basic Energy Sciences, Division of Chemical Sciences

radiation field [15]. The difference between the two processes lies in how the initial coherence is created [16]. Characteristic for both processes is that the emission is delayed with respect to the pump pulse and that the delay can be long compared to the pump pulse length. A prerequisite for these phenomena to occur is that the dephasing time is long compared to the time in which the atoms interact with each other, so that the coherence can be maintained. When these requirements are not satisfied, for example, in the presence of rapid dephasing collisions at elevated pressures, we are approaching a region in which stimulated emission or amplified spontaneous emission occurs [11]. Because the high pressure regime ($\gtrsim 10$ Torr) is usually encountered in diagnostic situations, we are most certainly in a regime where stimulated emission is responsible for the emission. A variety of other nonlinear optical processes such as four-wave mixing and stimulated hyper-Raman scattering [17] can also occur under these conditions, and can interfere with the stimulated emission process under some conditions [18, 19]; these processes are not treated in this paper.

In this paper we address some properties of the SE technique as a diagnostic tool, including experiments aimed at comparisons between LIF and SE, investigations of the influence of SE on quantitative LIF measurements, and possible extensions of the SE technique to obtain an increase in spatial resolution. The possibility of increasing the SE signal intensity, in both the forward and backward direction, by introducing optical feedback is of special interest. In most experiments we have chosen carbon monoxide as a test species because of the ease of using a stable gas for well controlled experiments, exciting the two-photon $B\,^1\Sigma^+ \leftarrow X\,^1\Sigma^+$ transition at 230 nm and detecting subsequent $B\,^1\Sigma^+ \rightarrow A\,^1\Pi$ emission in the blue-green region of the spectrum. Fluorescence emission from this process was first studied by Loge et al. [20], and later used for flame detection of CO [4]. Stimulated emission from this process was first reported in the paper describing the flame study [4], and has also been discussed by Tiee et al. [21]. In addition to the CO experiments, we also report some new measurements made on atomic oxygen.

Section 1 of this paper describes the experimental apparatus. During the course of these experiments we observed several differences between the behavior of the SE and LIF signals, in particular with respect to laser power dependences, spectral characteristics, spatial generation, and pressure dependences. These effects, and the possibility of probing the SE region to increase the spatial resolution of the signal, are reported in Sect. 2. We develop a semi-quantitative model to describe these observations in Sect. 3, followed by a conclusion.

1. Experimental Apparatus

We employed several different experimental arrangements during the course of the experiments; the most general set-up is shown in Fig. 1. The laser system consisted of a Nd:YAG laser, a dye laser, and frequency-doubling/mixing components. The Quantel YG 581-10 Nd:YAG laser produced 1.06-μm pulses with a duration of 13 ns and a bandwidth of about 1 cm^{-1}. These pulses were frequency-doubled to yield about 400 mJ/pulse at 532 nm, and used to pump a Quantel TDL-50 dye laser operated with a prismatic beam expander in the cavity, yielding a linewidth of about 0.08 cm^{-1}. In the CO experiments, the dye laser was operated at 587 nm using Exciton Rhodamine 610 dye. The dye-laser beam was frequency-doubled and then mixed with the residual laser beam at 1.06 μm in KDP crystals to yield up to 3.5 mJ/pulse at 230 nm, the two-photon absorption wavelength of CO. For two-photon excitation studies of atomic oxygen, the same laser system produced about 2.5 mJ at 226 nm. Power dependences were obtained using a variable attenuator that did not affect the size, modal structure, or direction of the laser beam (Newport Corporation Model 935-10).

All costudies were performed in a stainless-steel cell equipped with fused-silica entrance and exit windows, and a separate quartz window perpendicular to the beam for LIF studies. A HI-TEC Series F-100/200 thermal mass flow meter controlled the gas flow. Fused-silica slides were placed before and after the cell to investigate the effects of adding a small fraction of the stimulated-emission signal as feedback in the forward and backward directions; the slide marked Q_F added feedback to the forward-direction beam (the SE signal propagating in the same direction as the laser beam), and the slide marked Q_B added feedback to the backward-direction beam (the SE signal propagating in the opposite direction as the laser beam). The laser beam was focused into the cell by a fused-silica lens ($f = 200$ or 500 mm), and the SE signal was re-

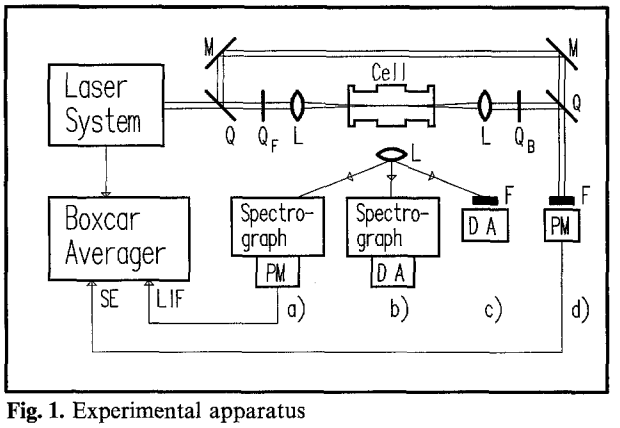

Fig. 1. Experimental apparatus

collimated with a similar lens ($f=200$ or 500 mm), spectrally isolated from the pump beam by a glass slide, and detected by a photomultiplier tube (EMI QB-9558, Fig. 1d). Operation of the PMT in a linear regime required attenuation of the SE signal (which in the case of CO was clearly visible by eye as a blue-green beam) by a factor of 10^6 with neutral density filters. In the LIF experiments, the fluorescence was imaged by a UV Nikon camera lens ($f/4.5$, $f=105$ mm) using one of three different detector arrangements a), b), and c) in Fig. 1. In the first two approaches, the LIF was imaged onto the entrance slit of a spectrometer (Jarrell-Ash 1233) containing three interchangeable gratings, yielding dispersions of 1.5, 6.0, and 24 nm/mm, respectively. Detector a) was a second EMI QB-9558 photomultiplier, and detector b) was a Tracor Northern TN-1710 multichannel analyzer with a diode array detector (Tracor Northern model 6144). The latter detector was also used in the imaging mode for spatially resolved measurements of fluorescence along the laser beam in the focal region, as represented by c). The LIF and SE signals from the two photomultipliers were transferred to a boxcar averager (PARC 4402) with two channels for simultaneous processing.

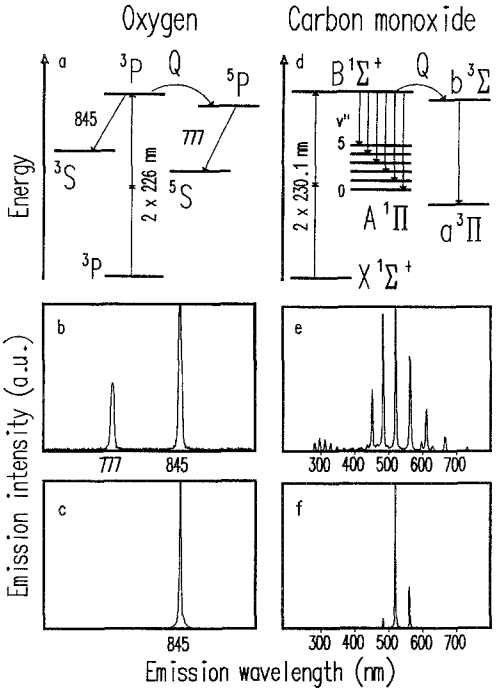

Fig. 2. a Atomic oxygen energy levels; **b** dispersed fluorescence spectrum of atomic oxygen; **c** dispersed SE spectrum of atomic oxygen; **d** CO energy levels; **e** dispersed fluorescence spectrum of CO; **f** dispersed SE spectrum of CO

2. Measurements

2.1. Spectral Measurements

One of the differences between the stimulated emission and the laser-induced fluorescence signals of O and CO was the spectral content of their emission. The relevant energy levels, the LIF spectrum, and the SE spectrum are shown in Fig. 2a–c for atomic oxygen and in Fig. 2d–f for CO. For atomic oxygen, the LIF spectrum displays both the triplet $3P$–$3S$ emission at 845 nm and the collision-induced quintet $3P$–$3S$ emission at 777 nm; in the SE spectrum, only the triplet emission at 845 nm appears. The absence of the 777-nm transition indicates that the laser pulse does not create a sufficient population inversion between the $3P$ and the $3S$ levels to reach the SE threshold (collisions transfer only a fraction of the $3P$ population to the $3P$ state).

The situation for CO is very similar. The LIF spectrum (Fig. 2e) is dominated by the $B\rightarrow A$ transitions between 480 and 725 nm, with smaller peaks around 300 nm originating from the collision-induced $b\rightarrow a$ triplet system. (The small peaks around 600 nm are the second order diffraction of this radiation.) We observed emission from the C_2 Swan bands, as reported in [4], but suppressed it by using a short gate (100 ns) on the diode array detector. The stimulated emission occurs on those transitions with the largest Franck-Condon factors in the $B\rightarrow A$ transition, as shown in Fig. 2f. We did not observe emission from the collisionally populated triplet system in the SE spectrum.

2.2. Power Dependences

We observe a distinct difference in the power dependences of the SE and LIF signals. This is because the SE and LIF processes do not have the same dependence on the density of excited species in the focal region of the laser beam. The strength of the LIF signal is proportional to the density of the excited molecules. The SE power dependence can be divided into three regions. First there is the region in which the excited state density is too low for stimulated emission to occur (below threshold). Next, a region of exponential gain is attained. Finally, a region of gain saturation is reached, where nearly all molecules are involved in the process, and the SE signal strength is limited primarily by the rate at which the atoms or molecules can be excited, leading to a signal dependence that is proportional to the density of excited molecules, similar to that for LIF.

The results of our SE power-dependence measurements on 76 Torr of CO are shown in log-log format in Fig. 3. We observe a threshold (not shown in the figure), followed by a region of very rapid gain (assumed to be exponential). The third region shows a linear dependence with a slope of about 1.5, which is lower than the expected quadratic dependence for a two-photon process, indicating the presence of other

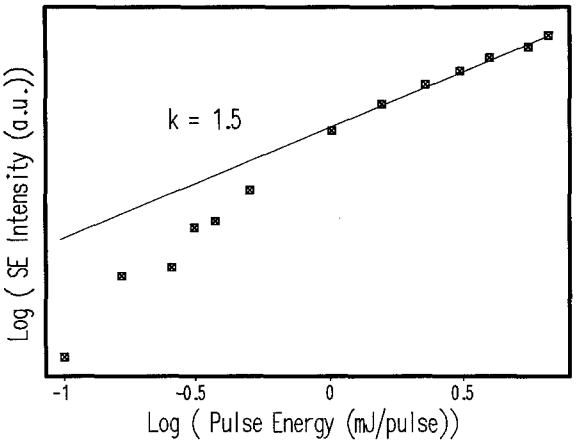

Fig. 3. Intensity dependence of the SE signal for 76 Torr of CO in the cell

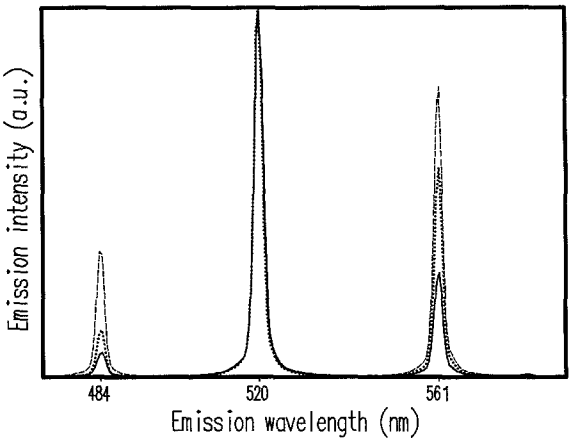

Fig. 4. Normalized SE spectra from CO in a cell without feedback (solid curve), with forward feedback (dotted curve), and with both forward and backward feedback (dashed curve)

processes (such as partial saturation of the two-photon transition and/or rapid photoionization out of the laser-excited state). In the absence of saturation and photoionization, we expect the SE signal to increase as the focal length of the focusing lens is decreased. However, we observe more intense SE using a 500-mm focal-length lens than using a 200-mm lens, probably because of increased photoionization for the shorter focal length (this point is discussed further in Sect. 2.7). In other two-photon-excited LIF studies, Loge et al. [20] report a slope of 1.2, and Tjossem and Smyth report a slope of 1.5 at low laser energies, decreasing to a slope near unity at higher laser energies [22].

2.3. *Feedback Studies*

We observed a considerable increase in the SE signal if a quartz plate was introduced prior to the cell and aligned so that optical feedback of the stimulated emission beam was achieved. It became evident that the increase in strength of the SE beam depended strongly on the laser power in the UV laser beam. In the case of CO this increase could be over two orders of magnitude if the laser power was set close to the threshold for stimulated emission, which, e.g., occurred at a laser power of 0.4 mJ and a cell pressure of 80 Torr using the 200-mm focal-length lens. However, the increase achieved at the threshold power exhibited strong fluctuations, indicating that it is sensitive to many parameters in the experimental set-up, such as the accuracy with which the feedback plate was aligned. If the laser power was set to its maximum value ($\sim$2 mJ/pulse in the cell), the increase was measured to be about a factor of four. This value for the increase was relatively independent of the position of the quartz plate along the laser beam for separations from the cell of up to 1 m.

The spectral content of the SE signal was observed to change when feedback was introduced into the system. Figure 4 displays three spectra, normalized to have equal peak heights on the strongest (520-nm) rovibronic transition. The solid curve displays the spectrum observed without any feedback (as in Fig. 2f). When the quartz plate prior to the cell was adjusted for forward feedback the spectrum with the dotted line was obtained; when the glass plate behind the cell was also adjusted for backward feedback (see below), the spectrum with the dashed line was recorded. Feedback evidently enhances the weaker rovibronic transitions relative to the strongest 520-nm transition, and this effect is accentuated in the presence of combined forward and backward feedback. This effect and the dependence of the gain on the laser power can be explained assuming that the stronger transitions saturate more easily than the weaker transitions as feedback is introduced and the SE signal becomes stronger.

2.4. *Spatial Resolution and* SE *Gain Probing*

For diagnostic purposes, one obvious disadvantage of the SE technique (compared to LIF, for example) is its limited spatial resolution along the laser beam due to its line-of-sight nature. In order to get a rough estimate of the spatial resolution, we translated a small atmospheric-pressure hydrogen-oxygen flame produced by a welding torch along the focal region of the laser beam, and measured the SE signal intensity from oxygen atoms as a function of traversed distance. Atomic oxygen is localized within the very thin ($<$1 mm) reaction zone of this flame. The conical cross-section of this flame means that the laser beam actually traverses two reaction zones and a region of unburned gases between them, yielding an effective structure approximately 3 mm in length. This structure was verified by imaging measurements of the LIF directly onto a diode-array detector. Using the 200-mm focal-length lens to focus the laser beam, the halfwidth of the SE distribution observed as the flame

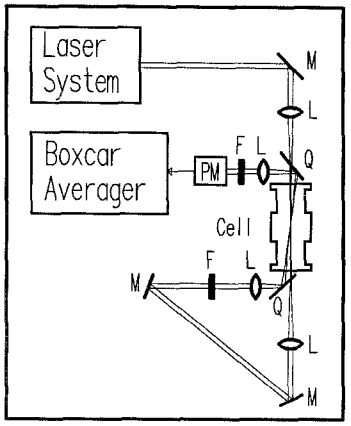

Fig. 5. Experimental arrangement for obtaining improved spatial resolution

was translated through the focal region was only about 4 mm, indicating that most of the SE is produced within a narrow region along the laser beam. This is not surprising because of the rapid decrease of the laser intensity with distance from the focal region and the nonlinear dependence of the SE signal on laser intensity.

Although the generation of most of the SE signal is confined to the beam waist, the situation is probably similar to colinear CARS (coherent anti-Stokes Raman scattering), which has insufficient spatial resolution for many applications. One concept for obtaining improved spatial resolution with SE detection is to use the SE beam after the cell as a probe beam, and to measure gain in this beam produced by the SE process. Using the experimental set-up shown in Fig. 5, the SE signal generated in the 76-Torr sample of CO was spectrally isolated from the pump laser as in the previous experiments. In this arrangement, however, the SE beam was reflected back into the probe area and crossed with the pump beam in a near-counterpropagating geometry at an angle of $\sim 6°$. The effect was investigated both with and without feedback from a quartz plate placed in front of the cell. The intensity of the probe beam was attenuated by the neutral density filters so that it would be amplified by the full unsaturated gain. Care was taken to make the beam waist of the longer-wavelength SE beam smaller than that of the pump beam to optimize the effect. We found that a gain of around 30% could be measured in the presence of forward feedback, which was ascertained by a slight misadjustment of the overlap.

2.5. *Forward and Backward Stimulated Emission*

Several experiments were performed to study the relative strengths of the SE signals emitted in the forward and backward directions. We first measured the ratio of the intensities of the forward and backward SE signals for various CO pressures, operating with 1–2 mJ/pulse, and using two different lenses to focus the laser beam (200 mm and 500 mm). During these experiments, the forward and backward SE signals were measured by the same PMT to assure a similar detector response. Care was also taken to provide identical optical losses along the beam paths, and to avoid possible polarization effects or spuriously scattered light. The two signal intensities were recorded by averaging over 1000 laser shots. Using the longer focal-length lens, the intensities in the forward and backward generated SE beam were found to be approximately equal. Using the shorter focal-length lens, we found that the SE signal generated in the backward direction was about a factor of two more intense than that generated in the forward direction. This factor seemed to be independent of pressure over the range 5–100 Torr, and relatively independent of pulse energy once the process was well above threshold. The difference in the behavior for the two focal-length lenses may be due to greater contributions of other nonlinear optical processes in the higher-intensity focal region of the shorter-focal-length lens.

We next investigated what gain could be achieved with forward and backward feedback of the SE. Operating at constant laser power and a CO pressure of 76 Torr, and alternately introducing feedback in the forward and backward directions, we found that the gain in the forward direction was approximately twice that in the backward direction. Folding in the factor-of-two difference in the two signal strengths observed without feedback, the net result with feedback is that the SE signal strengths in the forward and backward direction become roughly the same. This ratio was not affected by variations in laser pulse energy.

2.6. *Pressure Dependences*

CO was used as the test species in a comparison of the variation of the SE and LIF signal strengths as a function of pressure. The CO pressure in the cell was slowly increased from 0–760 Torr at a constant rate of about 0.2 Torr/s, and the SE (either with or without forward feedback) and the LIF signals were simultaneously measured using the two channels of the boxcar integrator. Figure 6 shows the LIF and SE signal strengths as a function of CO pressure in the cell (open circles and crossed squares, respectively), operating at a laser pulse energy of about 1.5 mJ/pulse. This figure also illustrates the change in the SE distribution when feedback was introduced (open squares). The LIF and SE signals behave very differently as the pressure is increased, with the SE signal increasing rapidly followed by an almost equally rapid decrease, while the LIF signal increases smoothly. The variation of the SE signal with pressure becomes less rapid in the presence

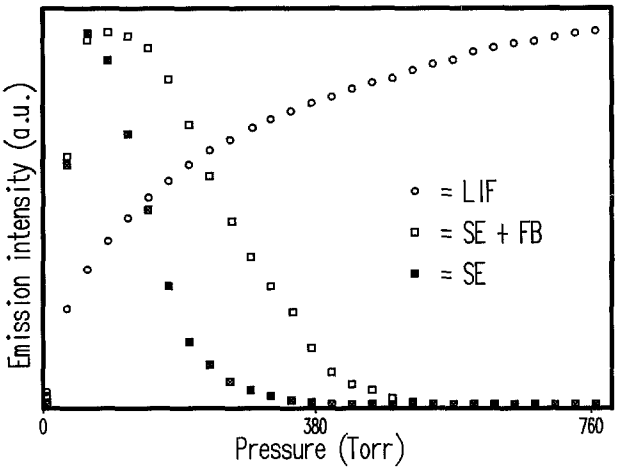

Fig. 6. LIF signals from pure CO as a function of pressure (open circles), and SE signals from pure CO as a function of pressure without feedback (crossed squares) and with feedback (open squares)

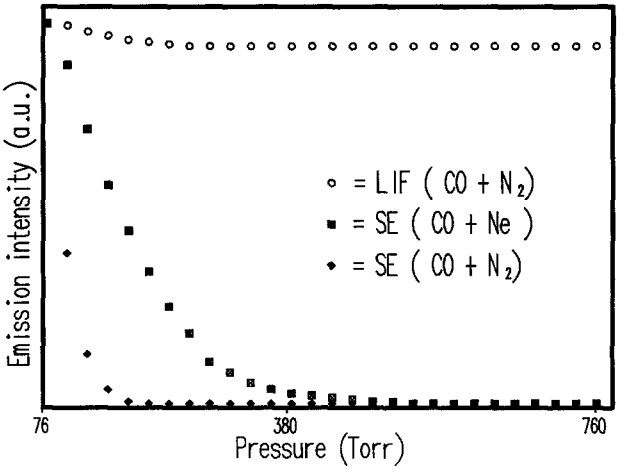

Fig. 7. Signal intensities from 76 Torr of CO as a function of added gas pressure: LIF signal intensity as function of added N_2 (open circles), and SE signal intensity as function of added Ne (crossed squares) and added N_2 (crossed diamonds)

of the forward-direction feedback, which seems very reasonable because the initial value of the stimulated emission rate is larger with seeding than without, allowing the stimulated process to build up.

Ne and N_2 were used as test gases to compare the effects of foreign-gas collisions on the SE and LIF signals to the behavior in pure CO. Figure 7 displays the results when an initial 76-Torr sample of CO was diluted with Ne or N_2 up to a total sample pressure of 760 Torr. Dilution by N_2 had almost no effect on the LIF signal either in the absence of feedback (open circles) or when feedback was present (not shown). The variation of the SE signal strength (without feedback) in the presence of added Ne and N_2 are represented by the crossed squares and crossed diamonds, respectively. The SE signal decreases less rapidly with added pressure of Ne than of N_2, consistent with LIF measurements [20, 23] indicating that Ne has a smaller quenching cross section than N_2 (although quenching may not be the most significant collisional effect). These points receive further attention in Sect. 3 of this paper.

2.7. Imaging Measurements and Effect of SE on LIF

In addition to its potential application as a diagnostic tool, it is also very important to determine if SE is in any way affecting the LIF signal by introducing a new physical process for depopulating the laser-excited electronic state. Because we are unable to directly turn on and off the SE process, our initial investigations were made by looking for changes in the LIF intensity and spectral content by modifying the strength of the SE signal, namely with and without optical feedback. We measured the LIF signal intensity while varying the laser pulse energy and the CO pressure in the cell, averaging 400 laser pulses for each set of conditions. As shown in Fig. 8a, the dispersed LIF spectrum with

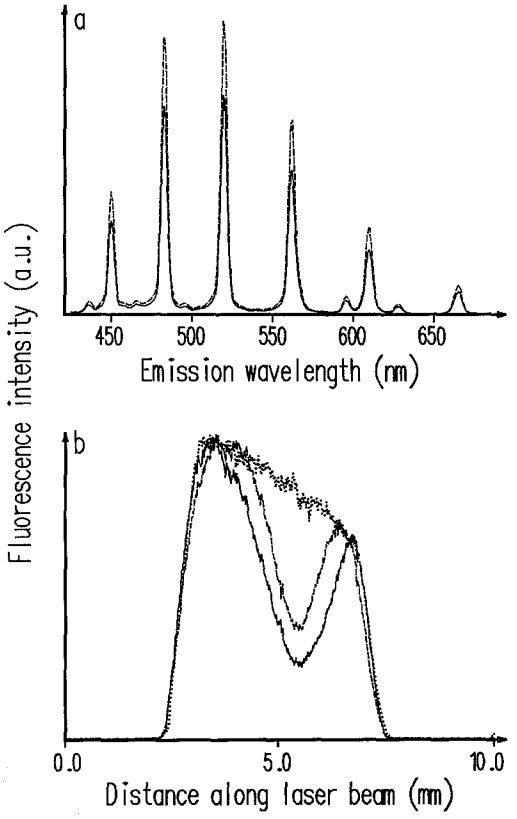

Fig. 8. a Dispersed spectra when using feedback for the SE signal (solid curve) and without feedback (dashed curve). **b** Normalized spatially resolved LIF distributions using the $f = 200$ mm focusing lens and a pressure of 76 Torr (solid curve) and 380 Torr (dashed curve). The spatially resolved LIF distribution at 76 Torr using the $f = 500$ mm focusing lens is illustrated by the dotted curve

feedback (solid curve) and without feedback (dashed curve) were spectrally identical; examination of the peak heights, however, demonstrates that enhancing the strength of the SE by adding the forward feedback could reduce the LIF signal strength by up to 25%. The magnitude of this reduction increased with laser intensity, but was independent of the CO pressure.

The spectra in Fig. 8a show that introducing feedback affected the LIF signal. They do not, however, tell us anything about the absolute scale of the influence of the SE on the LIF signal, namely the decrease of the LIF signal caused by the presence of SE in the absence of the feedback. We investigated this effect by imaging the LIF directly onto the diode-array detector, performing the measurements at two different CO pressures. As was shown in Fig. 6, there is a strong LIF signal at a CO pressure of 380 Torr, but the SE signal is zero. At a CO pressure of 76 Torr the SE signal is present, and could affect the spatial appearance of the LIF, especially if the SE signal strength is enhanced by introducing feedback. Accordingly, we imaged the LIF signal from the cell onto the diode array at the two pressures mentioned for two different focusing lenses and with forward feedback present.

The LIF image represented by the dotted curve in Fig. 8b was recorded using the 500-mm focal-length lens and a CO pressure of 76 Torr. In the absence of other effects, a flat-topped signal would be expected from the uniform CO distribution in the cell. The asymmetry in the image is primarily caused by nonuniform response across the detector, although there is also some contribution from attenuation of the laser beam by CO absorption (we found that the absorption grew quickly as the CO pressure was raised in the cell, reaching 70% at 760 Torr). The sharp cutoffs at the edges of the image are due to the size of the cell window.

The normalized curves obtained using the 200-mm focal-length lens at 76 Torr (solid curve) and 380 Torr (dashed curve) are shown in Fig. 8b. For these measurements, a large dip is observed in the middle of the LIF distribution. We believe that this decrease is caused by rapid photoionization in the focal region of the laser beam; a similar dip is not observed using the 500-mm focal-length lens (dotted curve) because the intensity in the focal region is lower. The asymmetry in the images is again caused primarily by nonuniform response across the detector. It is evident in Fig. 8b that the shape of the LIF images recorded using the 200-mm focal-length lens at the two pressures (solid and dashed curves) are different; we believe that this difference is caused by the presence of SE at 76 Torr, and its absence at 380 Torr. This difference occurs only in the inner part of the focus, which agrees with our contention that the extension of the SE focus is narrower than the LIF distribution because there is a threshold power density for stimulated emission.

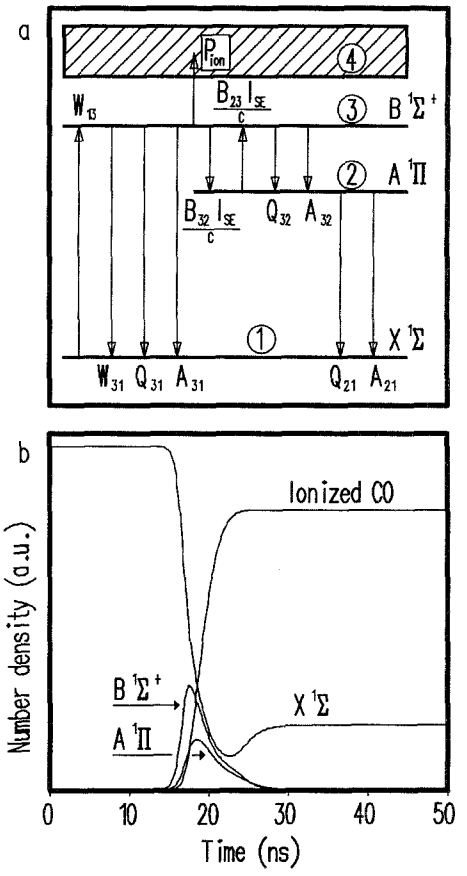

Fig. 9. a Schematic energy-level diagram for CO illustrating the important excitation and deexcitation routes. **b** Time-dependent solution to the CO rate-equation system in the absence of SE (500 Torr) calculated assuming a Gaussian laser pulse centered at $t=20$ ns and having a half-width of 5 ns

3. Discussion

In this section we develop a semi-quantitative model for the CO system, and use it to interpret the results presented in the preceding section. The most important characteristics of the CO system studied here are determined by a rate-equation analysis of the three-level system plus ionization continuum as illustrated in Fig. 9a. It should be pointed out that in studies on stimulated emission in oxygen [5], carbon [6, 12], and hydrogen atoms [7], the large-scale structure of the energy levels and the transitions are essentially the same as in the CO molecule. Even the relative relations of the rates in each of these systems are such that the semi-quantitative conclusions for CO obtained below are applicable for the other species as well. Models which exclude the influence of the stimulated emission, but otherwise are similar to the one described below, have been developed for carbon monoxide [24], oxygen [25], and hydrogen [26]. For carbon, Bergström et al. [12] have developed a quantitative computer model which includes spatial and temporal

variations of the laser pulse in the rate equation system. The results of their model agree with the results presented below.

For CO, levels 1, 2, 3, and 4 in Fig. 9a represent the $X\,^1\Sigma^+(v''=0)$ state, the $A\,^1\Pi$ state, the $B\,^1\Sigma^+(v'=0)$ state, and the ionization continuum, respectively. The system is characterized by the rate Eqs. (1–5):

$$\frac{dN_1}{dt} = -W_{13}N_1 + (A_{21}+Q_{21})N_2 + (W_{31}+A_{31}+Q_{31})N_3, \tag{1}$$

$$\frac{dN_2}{dt} = -([B_{23}I_{SE}/c]+A_{21}+Q_{21})N_2 + ([B_{32}I_{SE}/c]+A_{32}+Q_{32})N_3, \tag{2}$$

$$\frac{dN_3}{dt} = W_{13}N_1 + [B_{23}I_{SE}/c]N_2 - (W_{31}+P_{ion}+A_{31}+Q_{31}+[B_{32}I_{SE}/c] + A_{32}+Q_{32})N_3, \tag{3}$$

$$\frac{dN_{ion}}{dt} = P_{ion}N_3, \tag{4}$$

$$N_0 = N_1+N_2+N_3+N_{ion}, \tag{5}$$

where N_i is the population in level i, N_{ion} is the ionized population, N_0 is the total population, W_{13} is the two-photon absorption rate coefficient, P_{ion} is the photoionization rate coefficient, Q_{ij} is the quenching rate coefficient from state i to state j, $B_{ij}I_{SE}/c$ is the stimulated emission rate coefficient, and A_{ij} is the spontaneous emission rate coefficient. Equation (4) for the number of ions produced, N_{ion}, neglects recombination processes, which occur on a much slower time scale than the other processes considered here. For the discussion below it is useful to provide a very rough estimate of the approximate magnitude of the rate coefficients. The two-photon excitation rate for linearly polarized light may be estimated from the two-photon absorption cross section [21], α, of 1×10^{-30} cm^4/W. Although a wide range of laser pulse energies were used in the experiments, we will use typical data to make order-of-magnitude estimates, namely a laser pulse with an energy of 3 mJ in 5–6 ns focused with a 200-mm focal-length lens to a ~40-micron spot size, yielding a power density of approximately $I_{UV}=5\times10^{10}$ W/cm^2. Using $W_{13}=\alpha I_{UV}^2/h\nu$, where h is Planck's constant and ν is the frequency of the laser, the transition rate W_{13} is calculated to be $\sim1\times10^{10}$ s^{-1}. Measurements of the radiative lifetime of the $B\,^1\Sigma^+$ $(v'=0)$ state yielded $A_{32}=1.4\times10^7$ s^{-1} [27]. The quenching of $B\,^1\Sigma^+$ $(v'=0)$ has been measured at room temperature for carbon monoxide [20] $(6\times10^6$/Torr-s), neon [23] $(1\times10^5$/Torr-s), and nitrogen [20] $(5\times10^6$/Torr-s), leading to quenching rates of 1×10^7–5×10^8 s^{-1} at 100 Torr and an order of magnitude higher at atmospheric pressures. Predissociation can be neglected [22] for the $v'=0$ vibrational level in the $B\,^1\Sigma^+$ state. The $A\,^1\Pi$ state is characterized by quenching and emission rates which are comparable to or up to one order of magnitude larger than those for the $B\,^1\Sigma^+$ state [23]. The photoionization cross section σ_{ion} for $B\,^1\Sigma^+$ $(v'=0, J'=10)$ was determined by Ferrel [28] to be 1.4×10^{-20} cm^2 at 302 nm. Adopting this value for our 230–nm excitation wavelength yields a photoionization rate $P_{ion}=\sigma_{ion}I_{UV}/h\nu$ of approximately 1×10^9 s^{-1}. Finally, the average rate of the stimulated emission during the pump pulse was estimated from measurements of the intensity of the stimulated emission, ranging from 1×10^9–1×10^{12} s^{-1}. The rate varied strongly with laser power, CO pressure, etc., leading to the large range of observed rates. Although the stimulated CO signal was very strong, its energy in the absence of feedback was not more than a few μJ (i.e., a conversion efficiency of about 10^{-3}).

It is not possible to solve the rate-equation system, either under steady-state conditions or as a function of time, because it contains more unknowns (five) than useful equations (four). Equation (5), expressing number conservation, is degenerate with the first four and does not add any information. Several difficulties are encountered in attempting to complete the system by formulating a constitutive equation for the stimulated emission. In the absence of SE, the time dependence of the energy-level populations can be calculated independently at every point along the laser beam, and then summed to yield, for example, the total fluorescence. Figure 9b shows such a numerical solution to the rate-equation system, using rates taken from the text and adjusted for a pressure where no SE occurred (500 Torr). In the presence of SE, the situation is more complicated because different points are coupled to each other through the common radiation field, and are therefore no longer independent. Because the term $B_{ij}I_{SE}/c$ can be orders of magnitude larger than the other relaxation rates, erroneous predictions can result if it is neglected. For a more detailed study of SE and of fluorescence in a system in which SE occurs, a different theoretical approach is needed (e.g., the coupled-wave approach used to model second-harmonic generation and stimulated Raman processes), rather than one based on the simple rate equations typically used to describe LIF.

The high photoionization rate, in combination with the large two-photon absorption rate, ionizes a large fraction of the CO molecules in the beam in less than 1 ns. We thus conclude that the stimulated emission is a transient phenomenon. The importance

of the ionization is clearly shown in the calculation displayed in Fig. 9b, illustrating why the fluorescence intensity is lower near the focal region despite the higher two-photon excitation rate, and consistent with the dip observed in the fluorescence images shown in Fig. 8b. This is further illustrated in the fluorescence measurements where different gases were added as collision partners. Figure 7 shows the fluorescence intensity as a function of added N_2. Normally this fluorescence intensity is expected to obey a Stern-Volmer relationship $[(S=A_{32}/(A_{32}+Q_3)]$, where Q_3 (the total quenching rate out of level 3) is approximately [20] $5\times10^6\times p_{N_2}$. This theoretical relationship results in a much more rapid decrease of fluorescence intensity as a function of pressure than is observed experimentally. One possible reason is that there is an additional loss mechanism, in this case P_{ion}, which is larger than Q for the pressure range indicated. This would indicate a slightly higher ionization rate than calculated above.

The experiments depicted in Fig. 7 illustrate the sensitivity of stimulated emission to collisions of CO with foreign gases, and the insensitivity of LIF under the same conditions. Several factors contribute to the difference in the behavior of the SE and LIF signals. Because the spontaneous emission rate from the laser-excited state is independent of the (collision-broadened) linewidth of that transition, collisional broadening does not directly affect the LIF signal. The gain coefficient for stimulated emission is proportional to the lineshape of the transition, however; collisional broadening reduces the gain, and this reduction has a very large effect on the SE signal strength because the (unsaturated) signal is exponentially related to the gain coefficient [29]. In addition, several processes (Q_3, A_{32}) cooperate to equilibrate N_3 and N_2 after an inversion is created by the pump pulse, and BI_{SE} will not grow if the inversion is below threshold.

Figure 7 shows that relatively low pressures (e.g., $\sim$100 Torr of nitrogen) are sufficient to eliminate the stimulated emission in CO. This is in contrast to the stimulated emission from the detected atoms in flames, where the higher atomic two-photon-excitation and stimulated-emission cross sections (proportional to Einstein B coefficients) allow stimulated emission at atmospheric pressures [5, 6, 8]. Another difference between the atomic and molecular cases may relate to the validity of the three-level system described in this section, which ignores the presence of other atomic and molecular states. This approximation is reasonable for atomic systems, although quenching and spontaneous radiative decay to other levels may play some role. The three-level model is less likely to be accurate for describing molecular systems, especially at moderate pressures, where collisions can cause rapid redistribution among close-lying rotational levels. Such redistribution may explain the dramatic decrease of the SE signal with increasing pressure observed in Figs. 6 and 7 without a concomitant decrease in LIF signal. If collisions rapidly distribute the $B\,^1\Sigma^+$ population among rotational levels, the SE gain will become distributed among many rovibronic transitions, and the nonlinear nature of the gain process will cause the total gain to decrease rapidly. As we have observed, the behavior is very different for broadband LIF detection, for which collisional redistribution would not decrease the total signal from the linear fluorescence process.

The intensity of the stimulated emission beam in the backward direction was found to be equal to or larger than that in the forward direction for all experimental arrangements. This finding differs from the measurements reported in [21], in which the intensity was found to be a factor of ten larger in the forward direction than in the backward direction. This discrepancy may be due to varying roles of other nonlinear processes in the two experiments. Another possible explanation is the role of spiking in our laser pulse (due to longitudinal mode beating) in combination with the existence of a threshold for the stimulated emission. Measurements of these spikes using a streak camera indicate the presence of spikes on a subnanosecond time scale. With the rates discussed above, we find that when stimulated emission occurs, the rate is sufficiently high to equilibrate the inversion, thereby terminating the stimulated emission, within each spike. Thus each spike can be studied separately. If a photon is spontaneously emitted in the forward direction from the front end of a spike, it will not give rise to any gain because it is below threshold all the time while traveling with the pulse through the flame. However, if it is emitted in the backward direction, it will soon be in an area where the inversion is above threshold, and thus cause gain. Photons spontaneously emitted in the forward direction from the back of the spike will yield less gain because the backward propagating stimulated emission in combination with the photoionization has already depleted the inversion somewhat. This explains qualitatively the forward to backward intensity ratio in the absence of feedback. With forward and backward feedback, the forward to backward SE ratio was 1 : 1 (Sect. 2.5), which is reasonable because in this case the initial intensity at the SE wavelengths are above threshold for both directions.

In [21], introduction of feedback did not lead to any observable increase in the SE signal intensity; this fact was ascribed to delays before the feedback reached the CO cell that were comparable to their laser pulse duration ($\sim$4 ns). The presence of feedback effects in our studies can be explained by better temporal overlap between the feedback and the excitation pulse.

As described in Sect. 2.4, we found that the region which generates most of the SE signal has a rather narrow extension along the laser beam. It has also been shown that the gain of the ASE generated in a mirrorless laser with uniform inversion density is nonuniform [30], yielding an increased ASE spatial confinement even in a uniform medium [31]. This fact, combined with the use of a nonlinear (two-photon) excitation process in a focused geometry, indicates that moderate spatial resolution can be obtained using direct SE detection. For situations in which better spatial resolution is necessary, a crossed-beam configuration such as that described in Sect. 2.4 may be helpful. In future experiments with this geometry, it will be interesting to look for a possible loss in the backward beam and also a loss in the forward beam, as predicted by Allen et al. in ASE lasers [9]. One possible complication in the experiment we described, in which the probe beam was derived from the forward beam, is that a loss in the forward beam caused by an earlier (in time) section of the probe beam would result in a weakening of a latter section of the probe beam, reducing the net gain observed by integrating the entire probe pulse. This complication can be eliminated by using a second laser system, tuned to the wavelength of the SE, to provide the probe beam.

4. Conclusion

This paper describes several features of two-photon-excited stimulated emission, emphasizing its properties as a diagnostic tool. We attribute the process to stimulated emission rather than superradiance because it occurs in the regime of rapid collisional dephasing. The presence of a backward-direction signal argues against significant contributions from four-wave-mixing processes, which are only phase-matched in the forward direction. The sharp signal dependence on tuning to the atomic or molecular resonance suggest that stimulated hyper-Raman scattering is also not significant. (This interpretation is complicated by the differences between the "incoherent" SE process and the characteristics of the "coherent" resonant stimulated hyper-Raman processes; in particular, interferences with other nonlinear processes [18, 19] will affect the latter, but will not affect the former.) Many of the characteristics of SE can be explained by a simple model. However, to get a detailed understanding requires a model which incorporates spatial, temporal, and spectral variations, in combination with inclusion of photoionization, collisional effects, and spontaneous emission as well as possible influences from superradiance, stimulated hyper-Raman scattering, and four-wave mixing phenomena.

The SE technique possesses certain advantages over LIF, in particular the laser-like form that the signal takes. The generation of a signal in the backward direction can be especially useful for application that provide optical access in only one direction. The SE signal is very strong (visible by eye for CO and atomic hydrogen [7]), a characteristic which has made it possible to detect species which have not been detected in flames before, namely nitrogen [8] and carbon [6] atoms. There are, however, also disadvantages with the technique. It is a line-of-sight technique, providing less spatial resolution along the laser beam than can be obtained with LIF. We have demonstrated a crossed-beam configuration for obtaining improved spatial resolution, but implementation of this variation is not straightforward. The nonlinear dependence of the SE signal on number density, going from below threshold, to exponential to linear growth, makes quantitative measurements difficult to perform before a complete picture of the different processes described above has been achieved. In addition to its potential applications as a diagnostic tool, the other very important consideration that arises because of the generation of the SE signal is its possible influence on standard LIF measurements. The experiments described in this paper indicate that there can be an effect on LIF, as was also reported in [13]. The quantitative significance of this effect requires further investigation. We are currently pursuing these and other studies in our laboratories.

Acknowledgements. We are thankful to M. M. Fejer, S. Kröll, and R. E. Palmer for many stimulating discussions and helpful advice.

References

1. Alan C. Eckbreth: Laser Diagnostics for Combustion Temperature and Species (Abacus Press, Cambridge, MA 1987)
2. M. Aldén, H. Edner, P. Grafström, S. Svanberg: Opt. Commun. **42**, 244 (1983)
3. R.P. Lucht, J.T. Salmon, G.B. King, D.W. Sweeney, N.M. Laurendeau: Opt. Lett. **8**, 365 (1983)
4. M. Aldén, S. Wallin, W. Wendt: Appl. Phys. B **33**, 205 (1984)
5. M. Aldén, U. Westblom, J.E.M. Goldsmith: Opt. Lett. **14**, 305 (1989)
6. M. Aldén, P.-E. Bengtsson, U. Westblom: Opt. Commun. **71**, 263 (1989)
7. J.E.M. Goldsmith: J. Opt. Soc. Am. B **6**, 1979 (1989)
8. S. Agrup, U. Westblom, M. Alden: "Detection of Atomic Nitrogen using Two-Photon Laser-Induced stimulated Emission: Applications to Flames". Submitted to Chem. Phys. Lett.
9. L. Allen, G.I. Peters: Phys. Rev. **8**, 2031 (1973)
10. F.A. Korolev, V.V. Martynov, V.I. Odintsov, A.O. Fakhmi: Opt. Spectrosc. **40**, 600 (1976)
11. C. Cremer, G. Gerber: Appl. Phys. B **35**, 7 (1984)
12. H. Bergström, H. Hallstadius, H. Lundberg, A. Persson: Chem. Phys. Lett. **155**, 27 (1989)
13. M.B. Rankin, J.P. Davis, C. Giranda, L.C. Bobb: Opt. Commun. **70**, 345 (1989)

14. R.H. Dicke: Phys. Rev. **93**, 99 (1954)
15. M.S. Feld, J.C. MacGillivray: In *Coherent Nonlinear Optics*, ed. by M.S. Feld, V.S. Letokhov (Springer, Berlin, Heidelberg 1980) pp. 7–57
16. See, for example, Anthony E. Siegman: Lasers (University Science Books, Mill Valley, California 1986) pp. 547–551
17. Q.H.F. Vrehen, H.M.J. Hikspoors: Opt. Commun. **21**, 127 (1977)
18. R.W. Boyd, M.S. Malcuit, D.J. Gauthier: Phys. Rev. A **35**, 1648 (1987)
19. M.A. Moore, W.R. Garrett, M.G. Payne: Opt. Commun. **68**, 310 (1988)
20. G.W. Loge, J.J. Tiee, F.B. Wampler: J. Chem. Phys. **79**, 196 (1983)
21. J.J. Tiee, C.R. Quick, Jr., G.W. Loge, F.B. Wampler: J. Appl. Phys. **63**, 288 (1988)
22. P.J.H. Tjossem, K.C. Smyth: Chem. Phys. **91**, 2041 (1989)
23. F.J. Comes, E.H. Fink: Chem. Phys. Lett. **14**, 433 (1972)
24. J.M. Seitzman, J. Haumann, R.K. Hanson: Appl. Opt. **26**, 2898 (1987)
25. U. Meier, J. Bittner, K. Kohse-Höinghaus, Th. Just: Twenty-Second Symposium (International) on Combustion (Combustion Institute, Pittsburgh, PA 1989) pp. 1887–1896
26. J.T. Salmon, N.M. Laurendeau: Combust. Flame **74**, 221 (1988)
27. H. Bergström, H. Lundberg, A. Persson: "Investigations of stimulated emission on B–A lines in CO". Manuscript in prep.
28. W.R. Ferrell, C.H. Chen, M.G. Payne, R.D. Willis: Chem. Phys. Lett. **97**, 460 (1983)
29. A. Yariv: Quantum Electronics, second edition (Wiley, New York 1975) p. 162
30. R. Lang, P.L. Bender: Astrophys. J. **180**, 647 (1973)
31. L.W. Casperson: J. Appl. Phys. **48**, 256 (1977)